CHEMISTRY

Dual-color single-mode lasing in axially coupled organic nanowire resonators

Chunhuan Zhang,[1,2]* Chang-Ling Zou,[3]* Haiyun Dong,[1,2] Yongli Yan,[1,2] Jiannian Yao,[1,2] Yong Sheng Zhao[1,2]†

Miniaturized lasers with multicolor output and high spectral purity are of crucial importance for yielding more compact and more versatile photonic devices. However, multicolor lasers usually operate in multimode, which largely restricts their practical applications due to the lack of an effective mode selection mechanism that is simultaneously applicable to multiple wavebands. We propose a mutual mode selection strategy to realize dual-color single-mode lasing in axially coupled cavities constructed from two distinct organic self-assembled single-crystal nanowires. The unique mode selection mechanism in the heterogeneously coupled nanowires was elucidated experimentally and theoretically. With each individual nanowire functioning as both the laser source and the mode filter for the other nanowire, dual-color single-mode lasing was successfully achieved in the axially coupled heterogeneous nanowire resonators. Furthermore, the heterogeneously coupled resonators provided multiple nanoscale output ports for delivering coherent signals with different colors, which could greatly contribute to increasing the integration level of functional photonic devices. These results advance the fundamental understanding of the lasing modulation in coupled cavity systems and offer a promising route to building multifunctional nanoscale lasers for high-level practical photonic integrations.

INTRODUCTION

Miniaturized lasers have been demonstrated to be an important type of tool in a wide variety of fields, such as high-throughput chemical and biological sensing, color laser display, and on-chip optical communication and computing (1–5). The ever-increasing demand for information density and accuracy in highly integrated photonic devices calls for a nanoscale coherent light source capable of simultaneously achieving broadband output and good spectral purity with high stability, namely, multicolor single-mode nanolasers (6–9). Until now, the multiwavelength micro/nanolasers have been realized mainly through integrating several gain media with different bandgaps on single laser devices, for which the lasing wavelengths correspond to the fundamental bandgap energies of the respective materials (10–15). However, most of these multicolor lasers suffer from operating in multimode, originating from inhomogeneous gain saturation caused by spatial hole burning or cavity inhomogeneity (16). The presence of competing modes can lead to temporal fluctuations and false signaling (8, 9, 17), which has severely limited their practical implementation in various photonic devices.

To achieve single-mode lasing, several mode manipulation and selection strategies have been developed that make use of distributed feedback gratings (18), spatially varied optical pumping (19), and parity-time symmetry breaking (9, 17), among others. However, most of these single-mode lasers operate in only one gain region because these schemes cannot act on multiple wavebands simultaneously. Enlarging the free spectral range (FSR) through cavity size reduction is an effective approach to realizing single-mode lasing (20, 21), which is, in principle, applicable to different wavelengths concurrently but would markedly increase the lasing threshold. With one cavity applied as a spectral fil-

ter to the resonance modes of the other, a coupled cavity system could also enable the enlargement of FSR (22–25) while avoiding a significant increase of the threshold pump density. Meanwhile, the coupled cavity structure provides a potential possibility to achieve multiwavelength lasers by incorporating distinct optical gain media into the respective cavities. In active optical materials, organic categories with a large optical cross section and chemically tailorable optical properties (26–28) have been proven to be excellent gain media for laser action ranging from ultraviolet (UV) to near-infrared (29–31). Moreover, organic materials have an outstanding ability to self-assemble into well-defined low-dimensional structures that can function as optical microresonators (32). Because of the capability of simultaneously providing sufficient optical gain and feedback for the laser oscillations, the self-assembled nanostructures from organic molecules are promising candidates for constructing the heterogeneously coupled cavities.

Here, we demonstrate the realization of dual-color single-mode lasing based on a mutual mode selection mechanism in an optimized axially coupled cavity system, which is constructed through integrating two nanowire (NW) resonators self-assembled from distinct organic gain materials. The well-defined single-crystal NWs of two different organic compounds were synthesized through a liquid-phase self-assembly method. With smooth surfaces and flat end facets, the as-prepared NWs can serve as Fabry-Pérot (FP) cavities, providing sufficient feedback for the laser oscillations and thus allowing low-threshold multimode lasing at different wavelengths corresponding to the gain regions of the respective NWs. The two NWs were integrated to form an axially coupled heterogeneous resonator with a micromanipulator, leading to a significant mode selection effect. With large modulation of the threshold gain, the axially coupled heterogeneous cavities were proven both experimentally and theoretically to be an effective coupled structure for multicomponent mode selection. Under uniform excitation of the whole heterogeneously coupled cavities, dual-color lasing has been fulfilled from the distinct NWs based on a mutual mode selection effect. The end facets and the coupling gap of the heterogeneously coupled NW resonators can serve as nanoscale output ports and deliver different-colored coherent light signals, which could greatly

contribute to increasing the integration level of functional photonic devices. The results demonstrate a unique strategy for laser mode modulation in coupled cavities constructed via nanoarchitectonics and provide new insights into the construction of multicolor lasers with high spectral purity for ultradense photonic systems.

RESULTS

Figure 1 presents the diagram of the design principle for achieving dual-wavelength single-mode lasing. As shown in the top and middle panels, a single NW can synchronously provide the gain medium and serve as an FP cavity with the end facets of the NW constituting reflectors, for which optically pumped lasing action at different wavelengths can be readily achieved with output frequencies corresponding to the fundamental energy gaps of the respective homogeneous NW materials (33). Nevertheless, NW lasers usually operate in multiple modes arising from the native characteristics of simple FP cavities. Here, we propose a strategy to achieve dual-wavelength single-mode lasing through building axially coupled cavities with distinct NW materials, as depicted in the bottom panel of Fig. 1. Dual-color laser output might be realized from the distinct NWs under near-uniform excitation. Moreover, with each NW serving as a spectral filter to the resonance modes of the other in the coupled cavities, a two-color single-mode laser would be expected.

Cyano-substituted oligo(*p*-phenylenevinylene) (referred to as OPV-A; fig. S1) and cyano-substituted oligo-(α-phenylenevinylene)-1,4-bis(*R*-cyano-4-diphenylaminostyryl)-2,5-diphenylbenzene (referred to as OPV-B; fig. S2) were selected as the model compounds for the construction of the dual-wavelength NW lasers due to their excellent optical gain property at different wavebands and one-dimensional growth trend (34, 35). The detailed description of the synthesis procedures of the two OPV derivatives can be found in the Supplementary Materials. Figure S3 displays the fluorescence spectra of the OPV-A and OPV-B powders, with the maximum emission at ~460 and ~560 nm, respectively. The notable difference in wavelength is beneficial for separately studying the lasing characteristics of the two distinct OPV materials. These two compounds have excellent optical properties, with fluorescence quantum yields of 69.6 and 47.9% for OPV-A and OPV-B, respectively (fig. S4), which is essential for the optical gain and amplification (36).

The OPV-A and OPV-B NWs were fabricated via a liquid-phase self-assembly method (see Materials and Methods) (27, 37). Figure 2 (A and E) presents the fluorescence microscopy images of the OPV-A and OPV-B NWs, showing strong blue and yellow photoluminescence (PL), respectively. These as-prepared NWs exhibit typical features of an active optical waveguide, such as brighter spots at the wire ends and weaker PL from the wire bodies (38). The scanning electron microscopy (SEM) images (Fig. 2, B and F) show that both the OPV-A and OPV-B NWs have well-defined wire-like morphology, with smooth surfaces and flat end facets. With two flat end facets serving as mirrors, the NW can be treated as an FP cavity (39, 40), within which guided light reflects back and forth. The x-ray diffraction (XRD) measurements reveal the high crystallinity of the OPV-A and OPV-B NWs (fig. S5). The transmission electron microscopy (TEM) images and selected-area electron diffraction (SAED) patterns in Fig. 2 (C and G) indicate that the OPV-A and OPV-B NWs are single crystals growing along the [101] and [100] directions, respectively. The single-crystal nanostructures would exhibit excellent luminescence properties with very few defects in the material and facilitate optical waveguiding and confinement (41, 42). The optical propagation losses of the single-crystal NWs of OPV-A and OPV-B are as low as 0.0107 and 0.0071 dB/μm, respectively (fig. S6), which would contribute to the realization of low-threshold lasing oscillation. When the gain of the medium overcomes the loss of the cavity, the NW FP-type modes start to lase and generate coherent output (43).

Optically pumped lasing measurements were performed on a homebuilt far-field microphotoluminescence system (fig. S7). The NWs were nearly uniformly pumped by a pulsed laser beam (400 nm, 150 fs, and repetition rate of 1 kHz), whereby the beam waist was adjusted to be larger than the length of each NW. The PL spectra were recorded by collecting the light emission of the entire NW structures, unless stated otherwise. As shown in Fig. 2 (D and H), multimode lasing actions at ~464 and ~555 nm were observed in the OPV-A and OPV-B NWs, respectively. The PL images of the OPV-A and OPV-B NWs recorded above the lasing threshold (insets of Fig. 2, D and H) exhibit two impressive spots on the two end facets along the length of the NW, which is a typical characteristic of FP-type NW resonators (44, 45). Further investigation of the FSR in the PL spectra shows that the FSR is inversely proportional to the NW length (*L*), verifying the axially FP-type cavity resonances (fig. S8) (46).

For the FP-type oscillation, the lasing emission mainly outputs from the end facets of the NW materials. The head-to-head arranged NW structure would favor the strong coupling of the electromagnetic field (3, 8) while preserving the quality factor (*Q*) of the resonances. Accordingly, we designed and constructed a new type of axially coupled heterogeneous cavity through integrating the self-assembled
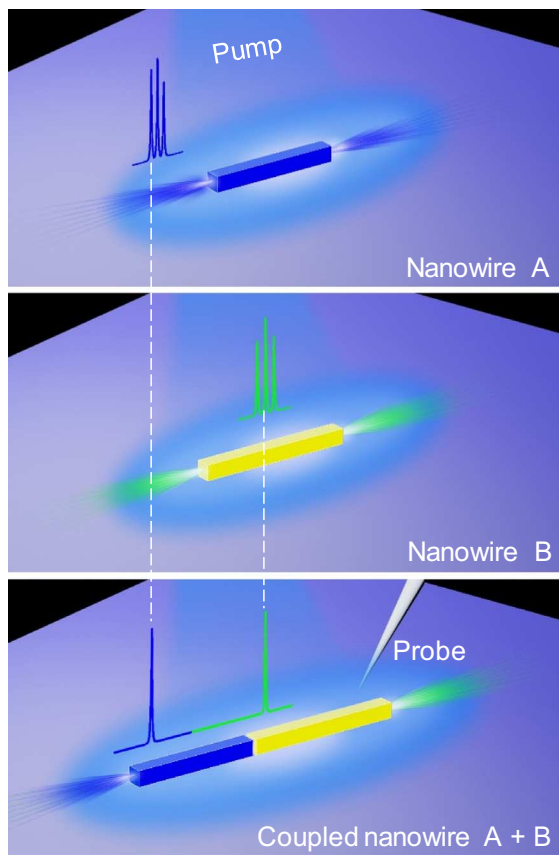

Fig. 1. Mutual mode selection concept in the coupled NW resonant cavities. Sketch of the multimode lasing from separate A and B NWs (top and middle) and dual-color single-mode lasing from axially coupled A + B NW cavities (bottom), where the NWs serve as both the laser source and the mode filter for each other.
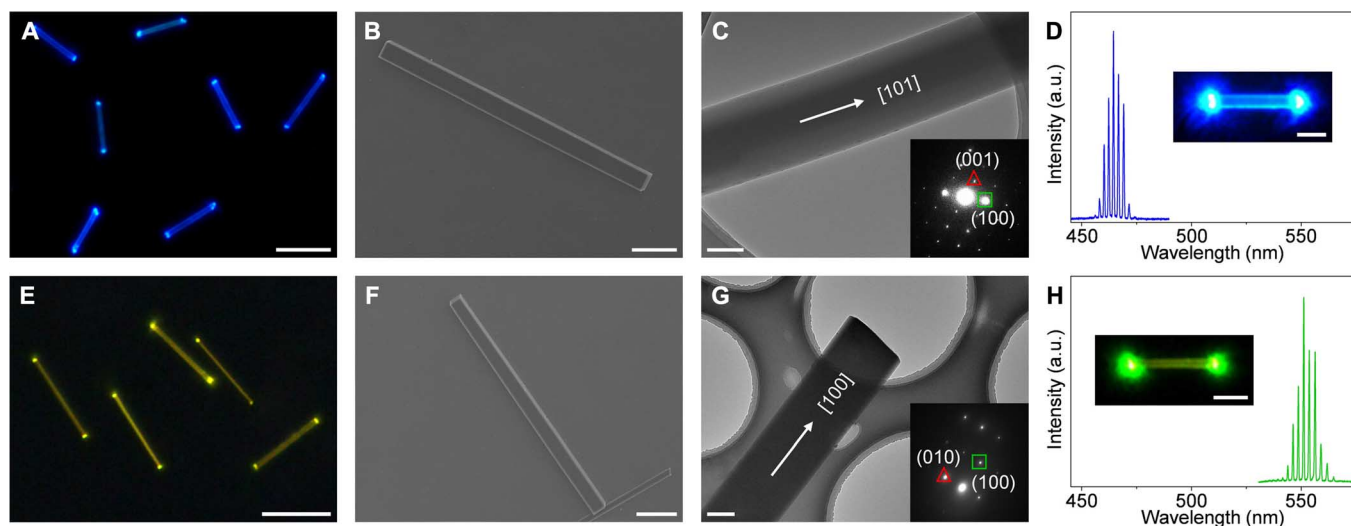
Fig. 2. Preparation of the OPV-A and OPV-B NW lasers. (**A** and **E**) PL images of the OPV-A and OPV-B NWs under UV (330 to 380 nm) excitation. Scale bars, 10 μm. (**B** and **F**) SEM images of the typical OPV-A and OPV-B NWs. Scale bars, 5 μm. (**C** and **G**) TEM images of the individual OPV-A and OPV-B NWs. Scale bars, 500 nm. Inset: SAED patterns of the NWs. (**D** and **H**) Multimode lasing spectra from the OPV-A and OPV-B NWs, excited with a pulsed laser (400 nm). Insets: Corresponding PL images of the OPV-A and OPV-B NWs above the lasing threshold. Scale bars, 5 μm. a.u., arbitrary units.

single-crystal OPV-A and OPV-B NWs to engineer the lasing spectrum properties of the individual NWs. Here, a micromanipulation method was applied to controllably fabricate such kind of heterostructures (figs. S9 and S10). Given that the fractional ratio between the NW lengths is critical for achieving single-mode operation in a coupled NW cavity system (8), the two-component NWs were controlled to have similar sizes, with a length ratio between 1:1 and 2:1, using a bend-to-fracture technique (47, 48). Moreover, the theoretical analysis (see the Supplementary Materials) indicates that the gap width needs to be ~0 to 400 nm, where effective optical coupling and mode modulation can be ensured. The axially coupled heterogeneous NWs with desired gap distances were constructed by alternately exerting a lateral force to the end of one NW in the micromanipulation process, as illustrated in fig. S13.

Figure 3A displays the PL image of the as-prepared axially coupled NWs under uniform excitation with the UV band (330 to 380 nm) of a mercury lamp; the NWs maintain the active optical waveguide property without evident scattering point along the NW body. This result indicates that the micromanipulation process introduced very little surface damage and contamination to the NWs, which is further supported by the SEM image shown in Fig. 3B. Therefore, the axially coupled heterogeneous NW resonators fabricated using the micromanipulation technique could well preserve the excellent optical properties of the individual NWs. The gap of the coupled NWs can be controlled to ~150 nm (inset of Fig. 3B), permitting effective optical coupling between the coupled NWs (8). This is confirmed by the experimental result that the PL of one NW can actively couple to the other one and output from the end facets (fig. S14).

To investigate the mode modification effect in the coupled NW resonators, we collected the lasing spectra of the OPV-A and OPV-B NWs with and without the coupling of the other distinct NWs. As shown in Fig. 3C, the OPV-A NW with a length of 12.4 μm exhibits a single-mode blue lasing output when axially coupled with an OPV-B NW (13.5 μm in length) (Fig. 3C, top), which is in sharp contrast with the multimode lasing action in the same isolated OPV-A NW (Fig. 3C, bottom). This clear mode selection effect can also be found in the OPV-B NW; that is, the laser output from the OPV-B NW with

a length of 21.7 μm changed from the multimode (Fig. 3D, bottom) to the single mode (Fig. 3D, top) when the single OPV-B NW was coupled with an OPV-A NW (18.9 μm in length).

In addition to the reduced number of lasing modes, the coupled heterogeneous NW structure did not cause an obvious increase of the lasing threshold, with the lasing thresholds of the OPV-A and OPV-B NWs in the coupled system being approximately 332 and 330 nJ/cm², respectively, slightly higher than those of the isolated ones (~254 and ~323 nJ/cm²) (Fig. 3, E and F). The thresholds of single-mode OPV-A and OPV-B NW lasers are lower than those of other single-mode NW lasers reported previously (18, 20–23, 49, 50), which can be ascribed to the intrinsic four-level system with large optical cross section in organic materials (32) and the coupled cavity nature. The pump power–dependent PL spectra are demonstrated in detail in fig. S15. Note that the heterogeneously coupled NW structures exhibit stable single-mode operation over a large range of pump intensities (fig. S15, B and D). This robust mode selection effect cannot be achieved in single FP-type NW cavities, where the single-mode operation is accompanied by a sharp increase of the threshold gain (20, 21).

A systematic investigation of the structural parameters, including NW length and intercavity gap distance, was performed to more comprehensively demonstrate the mode selection effect in the axially coupled heterogeneous NW resonators. In these structures, the active NW determines the mode frequencies, whereas the passive NW causes the mode selection effect. Therefore, the length of an individual NW has a great influence on the output mode of the coupled NW lasers. Here, we investigated the lasing properties of the same OPV-B NW coupled with OPV-A NWs of different lengths (fig. S16). Clear mode selection effect can be observed from all these coupled structures. The selected modes from the OPV-B NW varied because of the difference in threshold modulation provided by distinct OPV-A NWs. When a longer OPV-A NW was applied as filter cavity, more than one mode was selected from the OPV-B NW. This is because the longer filter NW supports more resonance modes, which leads to the simultaneous match of multiple modes between the lasing and filter cavities. Therefore, the NWs, with lengths in the range of ~10 to 25 μm, were suggested for

the realization of single-mode laser because they not only avoid the multimode selection but also provide sufficient optical gain.

The gap distance is another factor that strongly affects the mode selection effect in the heterogeneously coupled NWs. Here, we studied the evolution of the laser spectrum by gradually changing the gap distance of the heterogeneously coupled NWs. An OPV-B NW with a length of 17.2 μm was selected as the lasing cavity, whereas an OPV-A NW with a length of 24.8 μm was selected as the mode filter. As shown in fig. S17, the significant mode selection effect can be achieved in a large range of gap distance (~0 to 600 nm). When the gap width reaches ~900 nm, more modes began to emerge because of the decrease of optical coupling between the two NWs. With further increase of the gap distance over 1200 nm, there is no obvious mode selection effect any more. The range of gap distance for effective mode selection is as large as ~0 to 600 nm, which agrees with the theoretical results (see the Supplementary Materials).

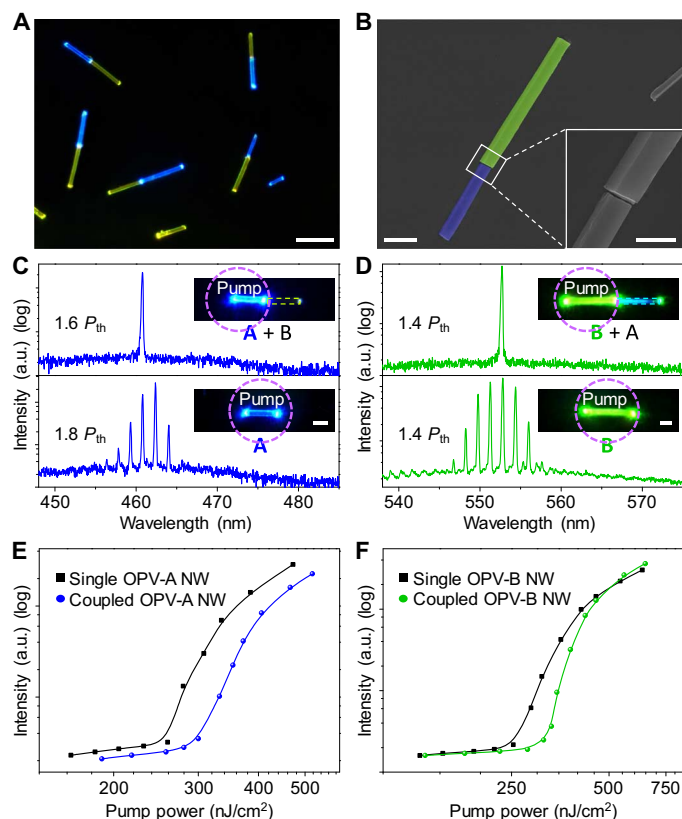The observed single-mode lasing in the coupled cavity system can be understood with a radiative coupling mechanism. As depicted in Fig. 4A, the light generated in the lasing cavity with gain medium can radiate to the free space from the end facet; part of the radiation can be subsequently coupled into the other cavity. Some of the light coupled to the external cavity will be reflected back to the lasing cavity and interfere with the originally reflected light at the end facet of the lasing cavity. When constructive interference occurs, the reflected light amplitude will be enhanced, resulting in a higher effective reflectivity. By contrast, the occurrence of destructive interference will reduce the amplitude of reflected light in the lasing cavity, corresponding to a lower effective reflectivity at the end facet. Thus, the passive cavity provides a wavelength-dependent reflectivity and functions as a filter for the lasing modes in the active one, which leads to the mode selection effect.

The NW end-facet reflectivity determines the quality factor of the cavity and the laser mode generation (32, 33). Here, we analytically calculated the effective end-facet reflectivity of the lasing cavity with and without the coupling of the filter cavity (see the Supplementary Materials) to better demonstrate the mode modulation mechanism. As plotted in Fig. 4B (black line), the calculated end-facet reflectivity (ρ) of the isolated NW is constant at different wavelengths. By comparison, the effective reflectivity (ρ_{eff}) of the lasing NW at the end facet coupled with the filter NW varies with wavelength periodically (Fig. 4B, red line) in the heterogeneously coupled cavity system. The wavelength-dependent end-facet reflectivity results in the mode modulation because the cavity modes with larger effective reflectivities are selectively amplified (51).

A more rigorous analysis can be performed by calculating the threshold gain of the cavity modes in the axially coupled heterogeneous NW laser (see the Supplementary Materials). For the isolated NW laser, the calculated modes have nearly equal threshold gain (Fig. 4C, black circle), whereby multiple modes are expected in the lasing output. In stark contrast, the threshold gain is modulated between different lasing modes in the coupled cavity structure (Fig. 4C,
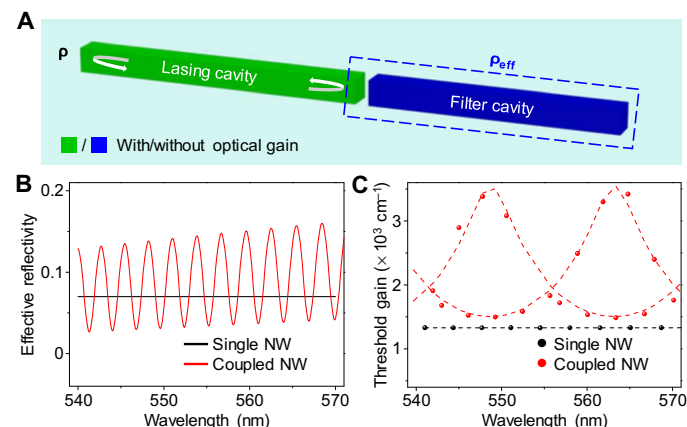

Fig. 3. Realization of single-mode lasing in heterogeneously coupled NWs. (**A**) PL image of the axially coupled heterogeneous NWs under uniform excitation with the UV band (330 to 380 nm) of a mercury lamp. Scale bar, 10 μm. (**B**) False-colored SEM image of the coupled NWs. Scale bar, 2 μm. Inset: Magnified view of the gap region. Scale bar, 1 μm. (**C** and **D**) Transition of the lasing spectra of the typical OPV-A and OPV-B NWs from multimode to single mode when they are coupled with each other. Insets: Corresponding PL images of the individual OPV-A and OPV-B NWs and the coupled NW pairs under laser excitation. Scale bars, 5 μm. (**E** and **F**) Pump power–dependent PL intensities of the isolated and heterogeneously coupled NWs shown in (C) and (D). The axially coupled heterogeneous NW cavity structure provides an effective mode selection effect while avoiding the significant increase of the lasing threshold.

Fig. 4. Mechanism of mode selection in the axially coupled heterogeneous NW resonator system. (**A**) Schematic illustration of the axially coupled heterogeneous cavities. ρ represents end-facet reflectivity of the single NW; ρ_{eff} represents effective reflectivity of the lasing cavity at the right end facet. (**B**) Effective reflectivity of the lasing cavity at the end facet coupled with the filter cavity, with the end-facet reflectivity of the isolated NW added as a comparison. (**C**) Threshold gain of the cavity modes in the active NW with and without the coupling of the passive NW. The modulated end-facet reflectivity and threshold gain demonstrate the mode selection mechanism in the axially coupled heterogeneous NW cavity system.

red circle), which resulted from the wavelength-dependent end-facet reflectivity. With a large modulation depth of the threshold gain, the axially coupled heterogeneous NW cavity structure supports a remarkable mode selection effect.

The experimental and theoretical results indicate that the mode selection mechanism in the heterogeneously coupled NWs can act on the gain regions of the two-component NWs concurrently. For a certain gain region, there is always one active cavity, with the other being passive. Each individual NW can serve as not only the laser source but also the mode filter for the other NW. As shown in the field intensity distribution profiles (simulated by the two-dimensional finite-element method) in Fig. 5A, there are two types of lasing modes with highest Q in the heterogeneously coupled cavity structure, with one dominating the left cavity and the other dominating the right. The mode field dominating the left NW can be modulated by the right NW cavity, and vice versa. This result fully demonstrates the mutual mode modulation effect in the heterogeneously coupled NWs, which holds the promise for achieving dual-color single-mode lasing.

This result is exactly what we have observed from the experiments. In the axially coupled heterogeneous NW resonators constructed with an OPV-A NW of 18.5 μm in length and an OPV-B NW (13.8 μm), both the OPV-A and OPV-B NWs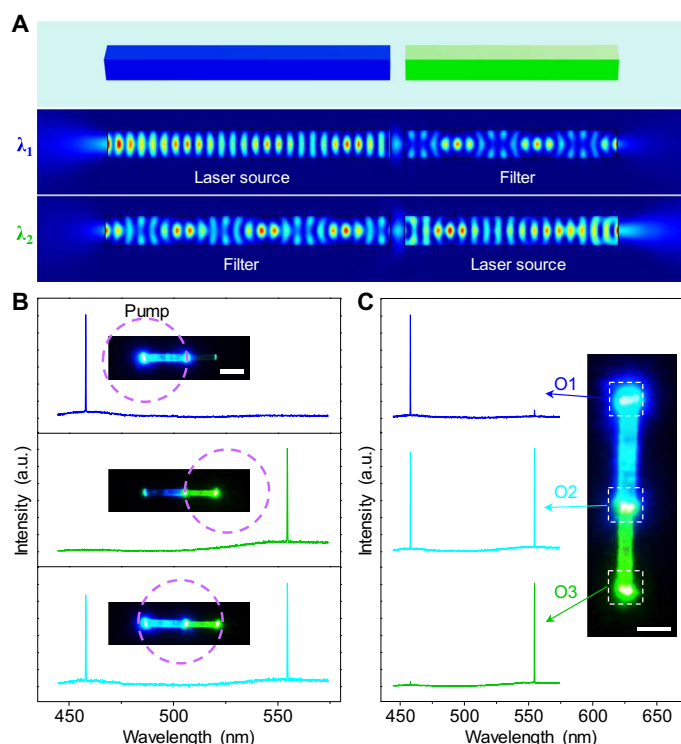 can output single-mode laser emissions in their respective gain regions, as shown in Fig. 5B (top and middle panels). Here, the OPV-B NW serves as the external modulator for the OPV-A active lasing cavity to generate the single-mode lasing at 458 nm, whereas their roles reverse for the generation of the single-mode laser at 554.5 nm. This mutual mode selection effect in the axially coupled heterogeneous NW cavities would enable the output of the dual-wavelength single-mode laser when the two coupled NWs are simultaneously used as both the active lasing cavities and the passive modulation cavities. As shown in the bottom panel of Fig. 5B, we have realized this expected dual-color single-mode lasing by pumping the heterogeneously coupled NW structure in whole. Such dual-color nanolasers with high spectral purity are particularly useful for light signal transmission and processing in parallel.

The efficient delivery of photons from light sources to miniaturized photonic circuits is central to various integrated photonic systems (52, 53). In our axially coupled heterogeneous NW resonator structures, the intercavity gap can serve as the outcoupling port of the dual-color single-mode laser emission, which is demonstrated in the middle panel of Fig. 5C (port O2). As illustrated in the simulated field distribution results in Fig. 5A, the two sets of laser mode fields are mainly distributed in the distinct NW components, which might result in the selective output of single-mode lasers with specific wavelengths from the end facets of OPV-A and OPV-B NWs. It can be observed from the outcoupled spectra in Fig. 5C that the blue single-mode lasing emission was especially output from the O1 port, whereas the green single-mode lasing was from the O3 port, which is desired for the full use of the advantages of multicolor lasers in photonic applications. These diverse coherent signals can be effectively delivered to the next-level photonic circuits by fabricating a passive near-field waveguide at the corresponding ports. The axially coupled heterogeneous NW cavities can synchronously deliver different coherent light sources from the nanoscale output ports, which would greatly contribute to increasing the integration level of functional photonic devices.

Fig. 5. Controlled outcoupling of the dual-color single-mode lasing from the coupled NW resonant cavities. (**A**) Simulated field intensity distribution of two types of highest-Q lasing modes in the axially coupled heterogeneous NW cavities, which manifests the mutual mode modulation effect in the coupled cavity. (**B**) Lasing emission spectra of the axially coupled heterogeneous NW cavities under laser excitation at different positions. The dual-color single-mode lasing was realized by pumping the heterogeneously coupled organic NW resonators in whole. Scale bar, 10 μm. (**C**) Spatially resolved PL spectra collected from three different ports: the intercavity gap of the heterogeneously coupled cavity system (O2) and the end facets of OPV-A (O1) and OPV-B (O3). Scale bar, 5 μm.

DISCUSSION

In summary, we have reported dual-wavelength single-mode lasing based on a mutual mode selection mechanism in axially coupled organic heterogeneous NW resonators. By integrating the two NWs self-assembled from different organic gain materials, an optimized axially coupled heterogeneous cavity system was constructed in which each individual NW functions as not only the laser source but also the mode filter for the other NW. With large modulation of the threshold gain, the heterogeneous structures were experimentally and theoretically proved to be a very effective coupled cavity system for multicomponent mode selection. Such a mechanism not only allows for achieving multicolor single-mode lasing but also permits the controllable outcoupling of the modulated lasers at nanoscale. The results demonstrated here give a comprehensive understanding of the connection between photonic functions and nanoarchitectonics, which provides new ideas for the construction of photonic elements with desired functionalities.

MATERIALS AND METHODS
Synthesis of material
Both the OPV-A and OPV-B NWs were prepared via the self-assembly of the molecules in the liquid phase by injecting 50 μl of the stock solution of OPV-A (5 mM) in tetrahydrofuran (THF) into 2 ml of hexane

and 15 µl of the THF stock solution of OPV-B (10 mM) into 2 ml of hexane, respectively. The rapid change of the solvent surroundings initiated the nucleation and self-assembly of OPV-A and OPV-B molecules. After aging for 7 min, many OPV-A NWs with regular morphology were obtained and dispersed in the colloid solutions. The OPV-B NW with regular morphology can also be found in the colloid solution after aging for 30 min. The colloid solutions were then used to prepare samples for further characterization and manipulation by drop-casting onto glass substrates. The as-prepared NWs have lengths of ~10 to 25 µm and cross-section widths of ~1000 to 2000 nm.

Morphological characterization
The morphology and crystallinity of the as-prepared OPV-A and OPV-B NWs were examined by SEM (Hitachi, S-4800), TEM (JEOL, JEM-1011), and XRD (PANalytical Empyrean).

Construction of coupled cavities
The micromanipulation of the NWs was carried out using a tungsten probe (size, 1 µm; Micromanipulator, model 7B-1), which was mounted on a precisely controlled three-dimensional moving stage, under an optical microscope equipped with a super–long-distance objective (20×; numerical aperture, 0.5). The NWs were cut to the desired length with a bend-to-fracture method when necessary. The detailed construction processes are presented in figs. S9 and S10.

Optical measurements
The fluorescence spectra were measured using a fluorescence spectrometer (Hitachi F-7000). The fluorescence quantum yields were measured by using the Hamamatsu Absolute PL Quantum Yield Spectrometer C11347. Bright-field optical images and fluorescence microscopy images were taken using an inverted fluorescence microscope (Nikon Ti-U) by exciting the samples with the halogen and mercury lamps, respectively. The optically pumped lasing measurements were carried out using a homebuilt far-field microphotoluminescence system equipped with a mode-locked Ti:sapphire laser, an inverted microscope, a charge-coupled device camera, and a spectrophotometer (fig. S7).

SUPPLEMENTARY MATERIALS
Supplementary material for this article is available at http://advances.sciencemag.org/cgi/content/full/3/7/e1700225/DC1

REFERENCES AND NOTES

1. M. H. Huang, S. Mao, H. Feick, H. Yan, Y. Wu, H. Kind, E. Weber, R. Russo, P. Yang, Room-temperature ultraviolet nanowire nanolasers. *Science* **292**, 1897–1899 (2001).
2. X. Duan, Y. Huang, R. Agarwal, C. M. Lieber, Single-nanowire electrically driven lasers. *Nature* **421**, 241–245 (2003).
3. B. Piccione, C.-H. Cho, L. K. van Vugt, R. Agarwal, All-optical active switching in individual semiconductor nanowires. *Nat. Nanotechnol.* **7**, 640–645 (2012).
4. F. Fan, S. Turkdogan, Z. Liu, D. Shelhammer, C. Z. Ning, A monolithic white laser. *Nat. Nanotechnol.* **10**, 796–803 (2015).
5. C. Zhang, C.-L. Zou, Y. Zhao, C.-H. Dong, C. Wei, H. Wang, Y. Liu, G.-C. Guo, J. Yao, Y. S. Zhao, Organic printed photonics: From microring lasers to integrated circuits. *Sci. Adv.* **1**, e1500257 (2015).
6. J. Xu, L. Ma, P. Guo, X. Zhuang, X. Zhu, W. Hu, X. Duan, A. Pan, Room-temperature dual-wavelength lasing from single-nanoribbon lateral heterostructures. *J. Am. Chem. Soc.* **134**, 12394–12397 (2012).
7. Z. Liu, L. Yin, H. Ning, Z. Yang, L. Tong, C.-Z. Ning, Dynamical color-controllable lasing with extremely wide tuning range from red to green in a single alloy nanowire using nanoscale manipulation. *Nano Lett.* **13**, 4945–4950 (2013).
8. H. Gao, A. Fu, S. C. Andrews, P. Yang, Cleaved-coupled nanowire lasers. *Proc. Natl. Acad. Sci. U.S.A.* **110**, 865–869 (2013).
9. L. Feng, Z. J. Wong, R.-M. Ma, Y. Wang, X. Zhang, Single-mode laser by parity-time symmetry breaking. *Science* **346**, 972–975 (2014).
10. Y. Ding, Q. Yang, X. Guo, S. Wang, F. Gu, J. Fu, Q. Wan, J. Cheng, L. Tong, Nanowires/microfiber hybrid structure multicolor laser. *Opt. Express* **17**, 21813–21818 (2009).
11. L. Cerdán, E. Enciso, V. Martín, J. Bañuelos, I. López-Arbeloa, A. Costela, I. García-Moreno, FRET-assisted laser emission in colloidal suspensions of dye-doped latex nanoparticles. *Nat. Photonics* **6**, 621–626 (2012).
12. F. Quochi, G. Schwabegger, C. Simbrunner, F. Floris, M. Saba, A. Mura, H. Sitter, G. Bongiovanni, Extending the lasing wavelength coverage of organic semiconductor nanofibers by periodic organic–organic heteroepitaxy. *Adv. Opt. Mater.* **1**, 117–122 (2013).
13. V. D. Ta, S. Yang, Y. Wang, Y. Gao, T. He, R. Chen, H. V. Demir, H. Sun, Multicolor lasing prints. *Appl. Phys. Lett.* **107**, 221103 (2015).
14. X. Zhuang, P. Guo, Q. Zhang, H. Liu, D. Li, W. Hu, X. Zhu, H. Zhou, A. Pan, Lateral composition-graded semiconductor nanoribbons for multi-color nanolasers. *Nano Res.* **9**, 933–941 (2016).
15. Q. Zhang, H. Liu, P. Guo, D. Li, P. Fan, W. Zheng, X. Zhu, Y. Jiang, H. Zhou, W. Hu, X. Zhuang, H. Liu, X. Duan, A. Pan, Vapor growth and interfacial carrier dynamics of high-quality CdS-CdSSe-CdS axial nanowire heterostructures. *Nano Energy* **32**, 28–35 (2017).
16. H. Zhu, Y. Fu, F. Meng, X. Wu, Z. Gong, Q. Ding, M. V. Gustafsson, M. T. Trinh, S. Jin, X.-Y. Zhu, Lead halide perovskite nanowire lasers with low lasing thresholds and high quality factors. *Nat. Mater.* **14**, 636–642 (2015).
17. H. Hodaei, M.-A. Miri, M. Heinrich, D. N. Christodoulides, M. Khajavikhan, Parity-time–symmetric microring lasers. *Science* **346**, 975–978 (2014).
18. L. Persano, A. Camposeo, P. Del Carro, V. Fasano, M. Moffa, R. Manco, S. D'Agostino, D. Pisignano, Distributed feedback imprinted electrospun fiber lasers. *Adv. Mater.* **26**, 6542–6547 (2014).
19. S. F. Liew, B. Redding, L. Ge, G. S. Solomon, H. Cao, Active control of emission directionality of semiconductor microdisk lasers. *Appl. Phys. Lett.* **104**, 231108 (2014).
20. Z. Yang, D. Wang, C. Meng, Z. Wu, Y. Wang, Y. Ma, L. Dai, X. Liu, T. Hasan, X. Liu, Q. Yang, Broadly defining lasing wavelengths in single bandgap-graded semiconductor nanowires. *Nano Lett.* **14**, 3153–3159 (2014).
21. W. Zhang, Y. Yan, J. Gu, J. Yao, Y. S. Zhao, Low-threshold wavelength-switchable organic nanowire lasers based on excited-state intramolecular proton transfer. *Angew. Chem. Int. Ed.* **54**, 7125–7129 (2015).
22. Y. Xiao, C. Meng, P. Wang, Y. Ye, H. Yu, S. Wang, F. Gu, L. Dai, L. Tong, Single-nanowire single-mode laser. *Nano Lett.* **11**, 1122–1126 (2011).
23. H. Xu, J. B. Wright, T.-S. Luk, J. J. Figiel, K. Cross, L. F. Lester, G. Balakrishnan, G. T. Wang, I. Brener, Q. Li, Single-mode lasing of GaN nanowire-pairs. *Appl. Phys. Lett.* **101**, 113106 (2012).
24. V. D. Ta, R. Chen, H. Sun, Coupled polymer microfiber lasers for single mode operation and enhanced refractive index sensing. *Adv. Opt. Mater.* **2**, 220–225 (2014).

25. J.-F. Ku, Q.-D. Chen, X.-W. Ma, Y.-D. Yang, Y.-Z. Huang, H.-L. Xu, H.-B. Sun, Photonic-molecule single-mode laser. *IEEE Photon. Technol. Lett.* **27**, 1157–1160 (2015).

26. I. D. W. Samuel, G. A. Turnbull, Organic semiconductor lasers. *Chem. Rev.* **107**, 1272–1295 (2007).

27. Y. Yan, Y. S. Zhao, Organic nanophotonics: From controllable assembly of functional molecules to low-dimensional materials with desired photonic properties. *Chem. Soc. Rev.* **43**, 4325–4340 (2014).

28. J. Gierschner, S. Varghese, S. Y. Park, Organic single crystal lasers: A materials view. *Adv. Opt. Mater.* **4**, 348–364 (2016).

29. Y. S. Zhao, A. Peng, H. Fu, Y. Ma, J. Yao, Nanowire waveguides and ultraviolet lasers based on small organic molecules. *Adv. Mater.* **20**, 1661–1665 (2008).

30. D. O'Carroll, I. Lieberwirth, G. Redmond, Microcavity effects and optically pumped lasing in single conjugated polymer nanowires. *Nat. Nanotechnol.* **2**, 180–184 (2007).

31. X. Wang, Q. Liao, H. Li, S. Bai, Y. Wu, X. Lu, H. Hu, Q. Shi, H. Fu, Near-infrared lasing from small-molecule organic hemispheres. *J. Am. Chem. Soc.* **137**, 9289–9295 (2015).

32. W. Zhang, J. Yao, Y. S. Zhao, Organic micro/nanoscale lasers. *Acc. Chem. Res.* **49**, 1691–1700 (2016).

33. S. W. Eaton, A. Fu, A. B. Wong, C.-Z. Ning, P. Yang, Semiconductor nanowire lasers. *Nat. Rev. Mater.* **1**, 16028 (2016).

34. Y. Li, F. Li, H. Zhang, Z. Xie, W. Xie, H. Xu, B. Li, F. Shen, L. Ye, M. Hanif, D. Ma, Y. Ma, Tight intermolecular packing through supramolecular interactions in crystals of cyano substituted oligo(*para*-phenylene vinylene): A key factor for aggregation-induced emission. *Chem. Commun.* **3**, 231–233 (2006).

35. Y. Li, F. Shen, H. Wang, F. He, Z. Xie, H. Zhang, Z. Wang, L. Liu, F. Li, M. Hanif, L. Ye, Y. Ma, Supramolecular network conducting the formation of uniaxially oriented molecular crystal of cyano substituted oligo(*p*-phenylene vinylene) and its amplified spontaneous emission (ASE) behavior. *Chem. Mater.* **20**, 7312–7318 (2008).

36. H.-H. Fang, J. Yang, J. Feng, T. Yamao, S. Hotta, H.-B. Sun, Functional organic single crystals for solid-state laser applications. *Laser Photon. Rev.* **8**, 687–715 (2014).

37. W. Yao, G. Han, F. Huang, M. Chu, Q. Peng, F. Hu, Y. Yi, H. Jiang, J. Yao, Y. S. Zhao, "H"-like organic nanowire heterojunctions constructed from cooperative molecular assembly for photonic applications. *Adv. Sci.* **2**, 1500130 (2015).

38. K. Takazawa, Y. Kitahama, Y. Kimura, G. Kido, Optical waveguide self-assembled from organic dye molecules in solution. *Nano Lett.* **5**, 1293–1296 (2005).

39. L. K. van Vugt, B. Piccione, C.-H. Cho, P. Nukala, R. Agarwal, One-dimensional polaritons with size-tunable and enhanced coupling strengths in semiconductor nanowires. *Proc. Natl. Acad. Sci. U.S.A.* **108**, 10050–10055 (2011).

40. Q. Zhang, G. Li, X. Liu, F. Qian, Y. Li, T. C. Sum, C. M. Lieber, Q. Xiong, A room temperature low-threshold ultraviolet plasmonic nanolaser. *Nat. Commun.* **5**, 4953 (2014).

41. Q. Bao, B. M. Goh, B. Yan, T. Yu, Z. Shen, K. P. Loh, Polarized emission and optical waveguide in crystalline perylene diimide microwires. *Adv. Mater.* **22**, 3661–3666 (2010).

42. N. Chandrasekhar, R. Chandrasekar, Reversibly shape-shifting organic optical waveguides: Formation of organic nanorings, nanotubes, and nanosheets. *Angew. Chem. Int. Ed.* **51**, 3556–3561 (2012).

43. J. Clark, G. Lanzani, Organic photonics for communications. *Nat. Photonics* **4**, 438–446 (2010).

44. J. C. Johnson, H.-J. Choi, K. P. Knutsen, R. D. Schaller, P. Yang, R. J. Saykally, Single gallium nitride nanowire lasers. *Nat. Mater.* **1**, 106–110 (2002).

45. H. Dong, Y. Wei, W. Zhang, C. Wei, C. Zhang, J. Yao, Y. S. Zhao, Broadband tunable microlasers based on controlled intramolecular charge-transfer process in organic supramolecular microcrystals. *J. Am. Chem. Soc.* **138**, 1118–1121 (2016).

46. X. Liu, Q. Zhang, Q. Xiong, T. C. Sum, Tailoring the lasing modes in semiconductor nanowire cavities using intrinsic self-absorption. *Nano Lett.* **13**, 1080–1085 (2013).

47. L. Tong, R. R. Gattass, J. B. Ashcom, S. He, J. Lou, M. Shen, I. Maxwell, E. Mazur, Subwavelength-diameter silica wires for low-loss optical wave guiding. *Nature* **426**, 816–819 (2003).

48. J. Li, C. Meng, Y. Liu, X. Wu, Y. Lu, Y. Ye, L. Dai, L. Tong, X. Liu, Q. Yang, Wavelength tunable CdSe nanowire lasers based on the absorption-emission-absorption process. *Adv. Mater.* **25**, 833–837 (2013).

49. Y. Xiao, C. Meng, X. Wu, L. Tong, Single mode lasing in coupled nanowires. *Appl. Phys. Lett.* **99**, 023109 (2011).

50. H. Xu, J. B. Wright, A. Hurtado, Q. Li, T.-S. Luk, J. J. Figiel, K. Cross, G. Balakrishnan, L. F. Lester, I. Brener, G. T. Wang, Gold substrate-induced single-mode lasing of GaN nanowires. *Appl. Phys. Lett.* **101**, 221114 (2012).

51. Y. Ma, X. Guo, X. Wu, L. Dai, L. Tong, Semiconductor nanowire lasers. *Adv. Opt. Photonics* **5**, 216–273 (2013).

52. H.-G. Park, C. J. Barrelet, Y. Wu, B. Tian, F. Qian, C. M. Lieber, A wavelength-selective photonic-crystal waveguide coupled to a nanowire light source. *Nat. Photonics* **2**, 622–626 (2008).

53. J. Ye, C. Zhang, C.-L. Zou, Y. Yan, J. Gu, Y. S. Zhao, J. Yao, Optical wavelength filters based on photonic confinement in semiconductor nanowire homojunctions. *Adv. Mater.* **26**, 620–624 (2014).

54. Z. Xie, B. Yang, L. Liu, M. Li, D. Lin, Y. Ma, G. Cheng, S. Liu, Experimental and theoretical studies of 2,5-diphenyl-1,4-distyrylbenzenes with all-*cis*- and all-*trans* double bonds: Chemical structure determination and optical properties. *J. Phys. Org. Chem.* **18**, 962–973 (2005).

55. F. He, L. L. Tian, X. Y. Tian, H. Xu, Y. H. Wang, W. J. Xie, M. Hanif, J. L. Xia, F. Z. Shen, B. Yang, F. Li, Y. G. Ma, Y. Q. Yang, J. C. Shen, Diphenylamine-substituted cruciform oligo(phenylene vinylene): Enhanced one- and two-photon excited fluorescence in the solid state. *Adv. Funct. Mater.* **17**, 1551–1557 (2007).

56. H. Dong, C. Zhang, X. Lin, Z. Zhou, J. Yao, Y. S. Zhao, Dual-wavelength switchable vibronic lasing in single-crystal organic microdisks. *Nano Lett.* **17**, 91–96 (2017).

57. A. V. Maslov, C. Z. Ning, Reflection of guided modes in a semiconductor nanowire laser. *Appl. Phys. Lett.* **83**, 1237 (2003).

58. S. Wang, Z. Hu, H. Yu, W. Fang, M. Qiu, L. Tong, Endface reflectivities of optical nanowires. *Opt. Express* **17**, 10881–10886 (2009).

Citation: C. Zhang, C.-L. Zou, H. Dong, Y. Yan, J. Yao, Y. S. Zhao, Dual-color single-mode lasing in axially coupled organic nanowire resonators. *Sci. Adv.* **3**, e1700225 (2017).